A lightweight and efficient portable soft exosuit for paretic ankle assistance in walking after stroke

Jaehyun Bae, Christopher Siviy, Michael Rouleau, Nicolas Menard, Kathleen O'Donnell, Ignacio Galiana, Maria Athanassiu, Danielle Ryan, Christine Bibeau, Lizeth Sloot, Pawel Kudzia, Terry Ellis, Louis Awad, Conor J. Walsh

Abstract— **Hemiparetic gait after stroke is typically asymmetric and energetically inefficient. A major contributor to walking deficits is impaired paretic ankle function. Impaired paretic ankle plantarflexion (PF) reduces forward propulsion symmetry and impaired paretic ankle dorsiflexion (DF) diminishes ground clearance during swing. We have developed soft wearable robots (soft exosuits) to assist paretic PF and DF during walking after stroke. Through experimental studies with poststroke patients, we have demonstrated that exosuits can improve forward propulsion symmetry and ground clearance in walking, ultimately reducing the metabolic cost of walking. This paper presents an optimized soft exosuit aimed at use in clinical gait training for patients poststroke. The optimized exosuit is lightweight, easy to don and doff, and capable of efficiently delivering mechanical assistance to the paretic ankle. This paper focuses on the optimized controller that can deliver well-timed consistent ankle assistance to patients. A preliminary study was performed using this exosuit with three poststroke patients with heterogeneous gait patterns. Results showed that compared to a previously published controller, more consistent assistive force profiles could be delivered to individuals poststroke while consuming 50% less electrical power. Additionally, a preliminary biomechanical assessment was performed during overground walking.**

I. Introduction

Stroke is a leading cause of long-term disability [1], with 80% of survivors having locomotor impairments [2]. Individuals after stroke typically present with hemiparetic gait, characterized as slow, asymmetric, and inefficient [3]–[5]. A major contributor to poststroke locomotion is impaired paretic ankle function, specifically during the push-off and swing phases of the gait cycle [5]–[9]. During push-off, diminished paretic ankle plantarflexion (PF) function inhibits the paretic limb's contribution to forward propulsion [6]–[8]. During swing, diminished paretic ankle dorsiflexion (DF) function leads to poor foot clearance [8], increasing the risk of tripping and falling [10].

Our laboratory has developed soft wearable robots, called soft exosuits, that deliver mechanical power to the lower-limb joints via the interaction of Bowden cables driven by actuators and functional apparel components [11]–[17]. Some of the exosuits were designed to augment walking and running in healthy individuals [11]–[15] and the others to enhance
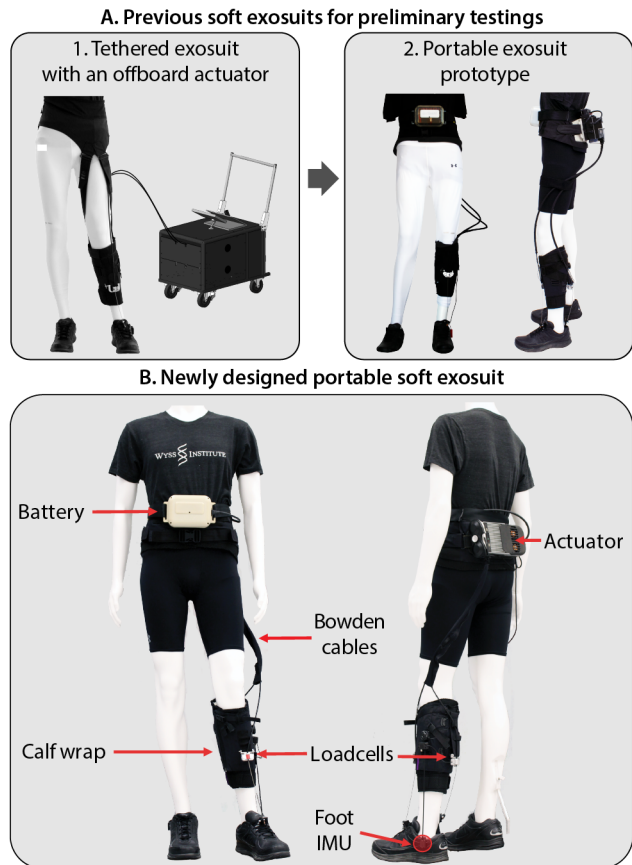

Figure 1. Soft exosuits for paretic ankle assistance in walking after stroke. (A) Two different exosuits were previously developed for preliminary tests. The first exosuit was a tethered system with an offboard actuator that allowed treadmill walking tests without adding extra mass from actuator and battery on wearer. The second system was a portable exosuit prototype for overground walking test. (B) A lightweight portable soft exosuit was newly developed for large-scale clinical research and practical use in clinics.

mobility and facilitate gait restoration in clinical populations [16], [17]. Specifically, exosuits for patients after stroke were developed to assist paretic ankle PF and DF during walking. The first exosuit prototype for paretic ankle assistance after stroke, which consisted of two apparel modules tethered to an offboard actuator, was developed for treadmill-based feasibility studies (Fig. 1a left) [16]. This initial work included

J.B., C.S., M.R., N.M., M.A., K.O., D.R., D.O., T.G.G., I.G., C.B., L.S., P.K., and C.J.W. are with the John A. Paulson School of Engineering and Applied Science and the Wyss Institute for Biologically Inspired Engineering, Harvard University, Cambridge, MA, 02138, USA.

L.A. and T.E. are with Department of Physical Therapy and Athletic Training, Boston University, Boston, MA, 02215, USA.

Corresponding author email: walsh@seas.harvard.edu (C.J.W.)

a gait event detection algorithm for pathological gait [16] and a force-based position controller that generated and adapted cable position trajectories based on force measurements [17]. With this tethered prototype, we showed that when comparing walking with the exosuit powered to unpowered, patients improved forward propulsion symmetry and ground clearance [17], reduced compensatory gait patterns [18], and eventually reduced the metabolic cost of walking [17], [19]. A first autonomous body-worn exosuit prototype (Fig. 1a right) was then developed to test the exosuit in overground walking [17]. This prototype employed similar control algorithms used in the tethered prototype, and produced similar outcomes to the treadmill-based tests in overground walking; specifically, patients improved forward propulsion symmetry and ground clearance when comparing walking with exosuit powered versus unpowered suit [17].

Although preliminary results were promising, exosuit prototypes were not optimized in terms of hardware and software, limiting use for overground gait training with multiple patients outside laboratory-oriented research. Specifically, tethered prototypes are not applicable to overground gait training and initial prototypes for of body-worn systems had not been optimized for weight, form factor, usability, comfort, serviceability, and power consumption. Moreover, due to fixed Bowden cable connections to the actuation system, cable length and routing were not reconfigurable for diverse patients with different body shapes and different affected sides. Additionally, the worn components took a long time to don and doff and adjust to the wearer and were non-washable.

In terms of software, the gait detection algorithm [16] was not robust enough in overground walking, as it relied on detecting heel strikes and the foot-flat phase of the gait cycle. However, patients poststroke may not walk with a heel strike, particularly in slow walking where many land with the mid-foot. Patients poststroke often employ "vaulting" compensations to alleviate foot drop [20], eliminating the foot-flat phase altogether. We also observed that the aforementioned force-based position controller [17] would not deliver consistent forces during overground walking due to increased gait variability compared to treadmill walking. A switching admittance-position controller [21] has been implemented with other exosuits for use in healthy populations, which has shown improved force consistency. However, this technique requires accurate human and exosuit models, which may not be available in poststroke populations due to the wide range of body types and heterogeneous gait patterns. Further, previous exosuit controllers were not optimized for cable slack management and electrical power consumption, important factors for in-clinic use.

To address these challenges that limited the suitability of the soft exosuit in overground gait training in a reliable and efficient manner, we developed an optimized portable exosuit and controller to assist paretic ankle PF and DF after stroke (Fig. 1b). System data (e.g. motor and sensor data) collected with previous prototypes informed the development of an improved actuation system that was greatly reduced in both mass and volume, while still maintaining capacity to deliver significant ankle assistance to a wearer. Functional apparel elements and integrated sensors were simplified for quick donning and doffing. The gait detection algorithm was improved in its robustness to gait patterns, no longer relying on foot flat and heel strike events. The force-based position controller was also improved to enable better force profile tracking while reducing electrical power consumption. We evaluated this optimized exosuit system in overground walking with three patients in chronic phase of stroke recovery.

II. SOFT EXOSUIT HARDWARE

The optimized soft exosuit to assist paretic ankle DF and PF comprises a waist belt that anchors an actuation system and a battery on the torso, two Bowden cables that connect the actuation system to the paretic ankle, a calf wrap that anchors the Bowden cable housings to the paretic shank, and an insole that anchors inner Bowden cables at the paretic foot (Fig 2). The total mass of the exosuit system is 3.8 kg, where its two heaviest components (actuator and battery) are worn close to body center of mass (COM), and only lightweight components such as a functional apparel and an insole are worn distally (See Fig 2 for component masses). As such, the system lessens its metabolic penalty to the wearer and adds minimal restrictions to the wearer's natural motion [22]. Additional modifications were made to the system components to reduce complexity and facilitate system setup in laboratories or clinics.

A. Functional apparel and insole anchors

New waist belt and calf wrap functional apparel components were designed for the exosuit system (Fig. 2). The waist belt includes a plastic plate with sliding connectors, with which an actuator can be easily secured to the back. A quick lacing mechanism (Boa Technology Inc, CO, USA) integrated into the calf wrap facilitates adjustability on a variety of calf shapes and sizes. Strain resistant textiles (Sailcloth, Dimension Polyant, USA) are integrated in the fabrication of the calf wrap to minimize deformation of the textile structure under load, and inner layers which directly make contact with wearer's skin are designed to be removable and washable to maintain hygiene between multiple users. Further, to fit a wide range of body shapes, multiple sizes of the waist belt and the calf wrap were fabricated (three sizes for waist belt, seven for the calf wrap). An insole with textile straps located anterior and

Figure 2. Exosuit hardware components and their masses

posterior to the ankle joint is placed in the shoe of the wearer's paretic foot. Connectors at the distal ends of inner Bowden cables attach to these textile straps. With inner cables connected to the insole and the cable housings connected to the calf wrap, the inner cable retraction driven by the actuator delivers mechanical power to the ankle.

B. Actuation system

The design of a two degree-of-freedom actuation unit and a pulley cartridge was informed by data collected from the previous exosuit actuation systems (Fig. 1A) [16], [17]. Design efforts focused on minimizing mass and volume while covering different body shapes and sizes and right and left paretic legs (Fig. 3). The assembly of actuation unit and pulley cartridge is 248 mm long, 135 mm tall, and 63 mm wide. With its narrow and compact design, the actuation system significantly reduced its effective inertia applied to the body COM. The actuation unit contains two motors (EC-4pole 22 90W, Maxon Inc, USA), gear boxes (GP 32 HP 123:1, Maxon Inc, USA), encoders (16 EASY, Maxon Inc, USA), and a custom-made electronics board using an Atmel processor (SAME70N21, Atmel Co, USA) and motor drivers (Gold Twitter, Elmo Motion Control Ltd, Israel). We chose 300 N as the maximum cable force requirement and 1.4 m/s as the maximum walking speed requirement, and collected actuation data at these operating conditions for multiple healthy individuals and patients poststroke with previous exosuit systems. The collected data was then used in combination with an analytical model of the actuation system, similar to that in [21], to predict the actuation and thermal performance of various potential motor and gear combinations. Based on simulation results and considering system mass and form factor, the motors and gear boxes listed above were selected.

The aforementioned actuation model was also used to derive the voltage, current, and power requirements of the power electronics. Motor drivers were therefore selected to be capable of 50 V and 60 A peak current, and the battery were selected to supply 48 V with 1450 mAh capacity, which makes the actuation system capable of assisting for more than 90 minutes of continuous active walking, sufficient for running a maximum-duration rehabilitation session without recharging or replacing the battery.

The actuation unit can be connected to different pulley cartridges with Bowden cables of different lengths. Based on the size of the subject, the correct cartridge with Bowden cables of the most appropriate length can quickly and easily be attached to the system. The correct sizing of Bowden cables is important to allow free motion of a wearer and minimize excessive cable slack. The use of reversible cartridges also enables the system to be easily configured for either left or right hemiparesis patients as shown in Fig. 3A.

C. Textile-integrated sensors

Load cells and inertial measurement units (IMUs) are integrated in the exosuit functional apparel components to enable a hierarchical closed-loop controller described in section IV. Specifically, two load cells (LSB200, Futek, USA) were integrated in the textile loops of the calf wrap to measure DF and PF forces generated by Bowden cable retractions. The force measurements are used in the cable position trajectory generator of the high-level controller (See section IV B and C). Additionally, IMUs (MTi-3, XSens, Netherlands) are mounted laterally on each shoe to measure foot angle and angular velocity. The IMU measurements are used in the gait detection algorithm (See section IV A).

III. MODELING EXOSUIT ON THE PARETIC ANKLE

To demonstrate how the functional apparel components and Bowden cables interact with the human body to deliver mechanical power to the paretic ankle, a simple model of the calf wrap worn on the shank was created (Fig. 4). In this model, the relationship of the suit-generated force (f_{suit}) and the deformation of suit textiles and human soft tissues (d_{suit}), called exosuit-human series stiffness (F_{stiff}), is described by a nonlinear spring with hysteresis that presents different mechanical behaviors in loading and unloading [12], [23]. Specifically, two different positive monotonic functions describe loading and unloading behavior separately. Suit deformation occurs (i.e. d_{suit} becomes positive) when the inner cable length (d_{cable}) is shorter than the distance between two points fixed on the shank and foot (d_{ankle}, see Fig. 4). The fixed points are located where Bowden cable anchor points on the foot and the shank are in an undeformed exosuit. The distance d_{ankle} captures the ankle movement when force is not applied by the suit. When d_{cable} is longer than d_{ankle}, the cable is slack and the suit remains unchanged. Altogether, the ankle torque generated by the suit (τ_{suit}) can be described as follows:

$$d_{ankle} = d_0 - r_{ankle} \cdot \Delta\theta_{ankle} \qquad (1)$$

A   **Actuation system configuration for right hemiparesis**

Heatsink fins   Spline gear shafts   Inner cables connected to pulleys

Blower fans   **Actuation unit**

Configuration for left hemiparesis

Actuation unit is flipped 180°

Cable housings connected to cartridge   Thumb screw

Pulley cartridge

B   Air intake   Heatsink fins   Air exhaust

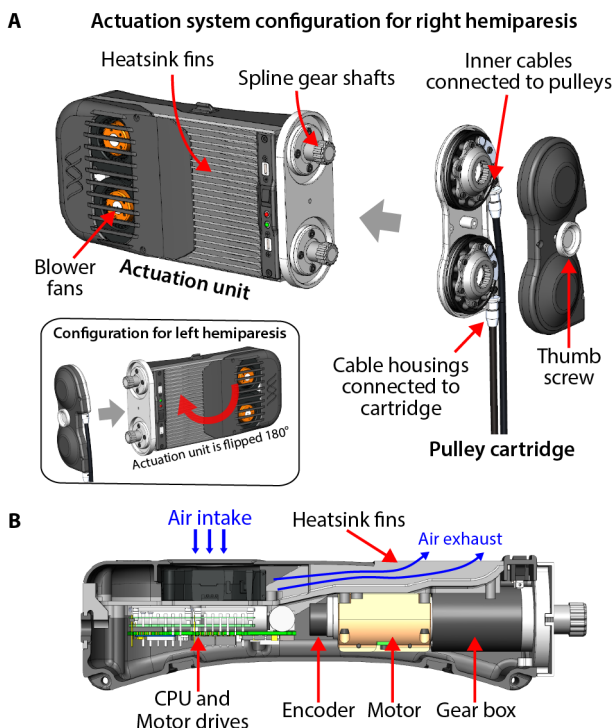CPU and Motor drives   Encoder   Motor   Gear box

Figure 3. Diagram of actuation unit and pulley cartridge. (A) The actuation unit and pulley cartridge are easily assembled with a thumb screw and can be configured for patients with right hemiparesis (main figure), or ones with left hemiparesis (small window). The motors are coupled to the pulleys through the use of spline gear shafts. (B) A section view of the actuation unit shows the internal system hardware. The motors and motor drives are thermally grounded to the aluminum chassis which supplies rigidity to the system and transfers the generated heat to the integrated heatsink fins.
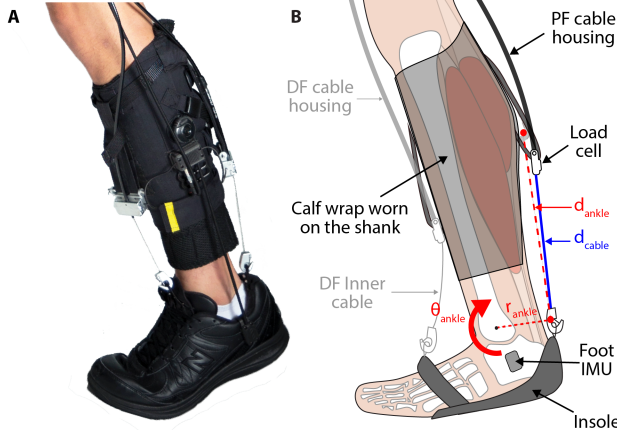
Figure 4. Picture (A) and diagram (B) of a paretic ankle wearing the soft exosuit. Two red points in the diagram illustrate Bowden cable anchor points when the suit is not stretched, which define d_{ankle}. The diagram highlights only PF cable actuation for simplicity.

$$d_{suit} = \begin{cases} d_{ankle} - d_{cable} \ , & d_{ankle} \geq d_{cable} \\ 0 \ , & otherwise \end{cases} \quad (2)$$

$$f_{suit} = F_{stiff}\left(d_{suit}, \mathrm{sgn}(\dot{d}_{suit})\right) \quad (3)$$

$$\tau_{suit} = r_{ankle} \cdot f_{suit} \quad (4)$$

where d_0 is the distance between the cable anchor points when the ankle is in a neutral position, $\Delta\theta_{ankle}$ is the ankle angle change from the neutral position, and r_{ankle} is the cable moment arm with respect to the ankle (see Fig. 4). The stiffness model F_{stiff} depends on the direction of the change in d_{suit} due to hysteresis. Further details on F_{stiff} can be found in [12]. F_{stiff} may vary across wearers because of variation in body properties, such as the thickness of soft tissues and size of calf muscles. Note that this approach can be used to describe both PF and DF actuation.

IV. CONTROLLER IMPLEMENTATION

A hierarchical controller that consists of two nested control loops was implemented to generate consistent DF and PF force profiles at the appropriate timing during the gait cycle (Fig. 5). The outer layer, a high-level controller, detects key events in the gait cycle based on foot IMU measurements (gait event detection algorithm), and generates desired cable position trajectories based on the gait events and cable force measurements from load cells (cable position trajectory generator). The inner layer, a low-level controller, runs closed

loop control on motor position for the actuation system to track the desired cable position trajectories generated by the high-level controller. The low-level position controller comprises two cascading loops in which outer position loop generates desired velocity (v_{des}) based on position error (p_{err}), and inner velocity loop regulates control effort (u_{com}) to actuation system based on velocity error (v_{err}). This section focuses on describing the high-level controller. Further details about the low-level controller can be found in [21].

A. Gait event detection algorithm

A new gait event detection algorithm that detects paretic and nonparetic toe-offs (PTO and NTO) and nonparetic mid-swings (NMS) based on the sagittal plane foot IMU measurements was implemented (Fig. 6). This algorithm differs from previous gait event detection algorithms [16] in that it does not detect heel strikes and foot flat phases, instead detecting NTO, PTO, and NMS. With this approach, the new algorithm can be used not only for poststroke patients with mild gait deficits, presenting clear and consistent trends in IMU measurements, but also for patients with severe gait deficits who present diminished heel strike and foot flat phase (see graphs in Fig. 6).

To develop this new algorithm, we first sought consistent features in foot IMU measurement across various poststroke walking patterns. By examining data from our previous studies [17], we identified that sagittal plane foot angular velocities consistently presented negative peaks, then changed direction at toe-off, a feature appearing in both the paretic and nonparetic side, as shown in Fig. 6. Similar observations can be found in [24]. Also, sagittal plane nonparetic foot angles presented a consistent and monotonic increase during swing. Based on these observations, we designed a new gait event detection algorithm focused on detecting the negative peak in the sagittal plane foot angular velocity at toe-off and the mid-point of monotonic increase of the sagittal plane nonparetic foot angle during swing. Using the gait events detected with this algorithm, the gait cycle can be segmented into three distinct phases (P1-P3 in Fig 6): P1 is a paretic mid-stance phase (from NTO to NMS); P2 comprises a paretic terminal stance and pre-swing (from NMS to PTO); Last, P3 comprises a paretic swing and paretic weight acceptance (from PTO to NTO).

B. PF cable position trajectory generator

A force-based PF cable position trajectory generation algorithm was implemented to consistently deliver PF force
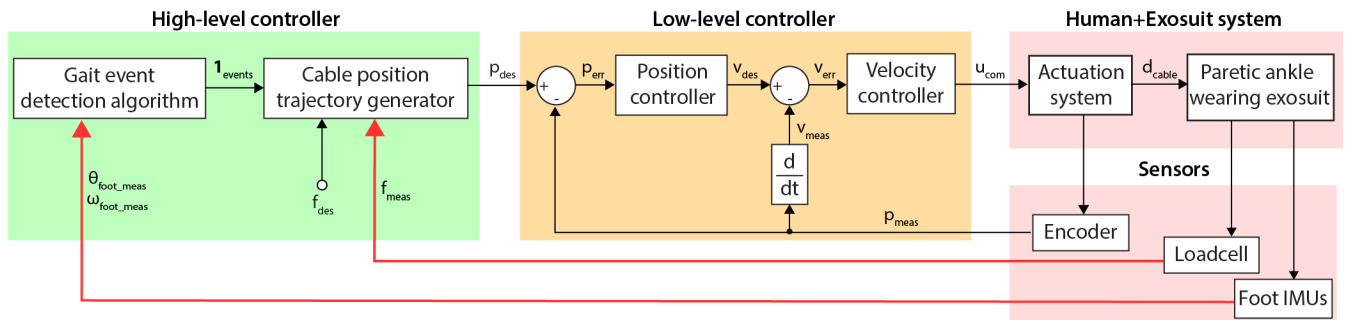

Figure 5. Schematic block diagram of exosuit controller. The diagram presents exosuit hardware (red), low-level controller (orange), and high-level controller (green). The high-level controller consists of a gait event detection algorithm that detects gait events based on foot IMU measurements (θ_{foot_meas}, ω_{foot_meas}), and a cable position trajectory generator that generates desired cable position (P_{des}) based on the gait events and force measurements (F_{meas}). The low-level controller regulates control effort (u_{com}) for actuator system to track the desired position generated by high-level controller.
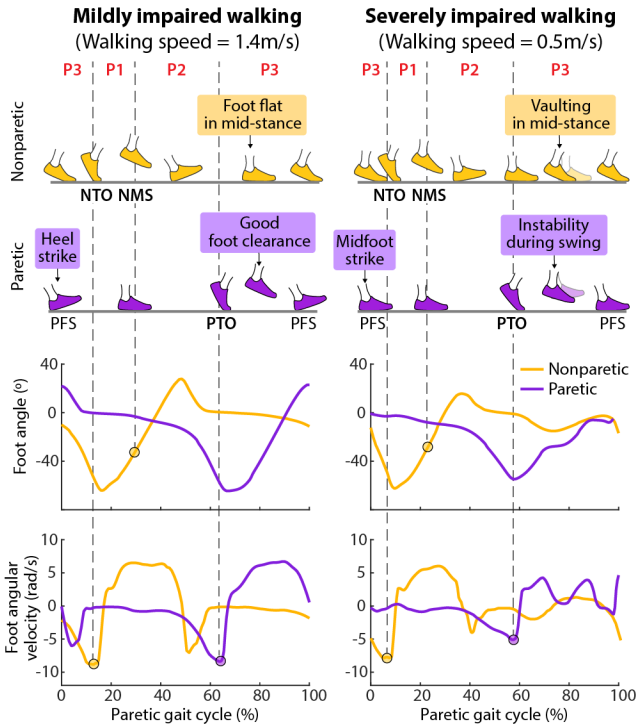
Figure 6. Sagittal plane foot trajectories and foot IMU measurements during the paretic gait cycle, a time period between two consecutive paretic foot strikes (PFS). The new gait detection algorithm detects paretic and nonparetic toe-offs (PTO and NTO) and nonparetic mid-swing (NMS) based on the sagittal plane foot angle and angular velocity measured by foot IMUs. The algorithm can robustly detect PTO, NTO, and NMS in poststroke patients with mild gait deficit (left) and severe gait deficit (right), and segment the gait cycle into three phases (P1- P3).

to the paretic ankle at appropriate timings (Fig. 7). The main goal was to generate PF cable force that has an onset at the end of paretic mid-stance, reaches a desired peak force (f_{des}) and diminishes before the beginning of the paretic swing phase. Our previous studies have validated that this form of PF force profile can improve forward propulsion symmetry and gait mechanics for patients after stroke [17], [19]. The second goal was to reduce motor power consumption by designing the position trajectory to reduce motor velocity and range of motion. To this end, the position trajectory generation algorithm adapts multiple cable position and velocity variables once per each walking stride (~1 Hz), and also adapts cable velocity iteratively per each control loop (1 kHz) when the cable retracts to give rise to the PF force.

Specifically, this algorithm adapts a position variable called baseline cable position (p_{base}) and three velocity variables consisting of pretension velocity (v_{pret}), initial pull velocity (v_{pull_i}), and pushout velocity (v_{push}) once per each walking stride identified by the gait detection algorithm. p_{base} is a cable position when force does not generate in the Bowden cable. v_{pret} is an average cable velocity in P1 when the cable starts to retract to onset PF force. v_{pull_i} is a cable velocity at NMS, a desired force onset timing since NMS coincides with the end of paretic mid-stance. v_{push} is a cable release velocity when the force ramps down. The velocity variables adapt in a same manner as follows:

$$v(n) = v(n-1) + k \cdot f_{err}(n-1) \qquad (5)$$

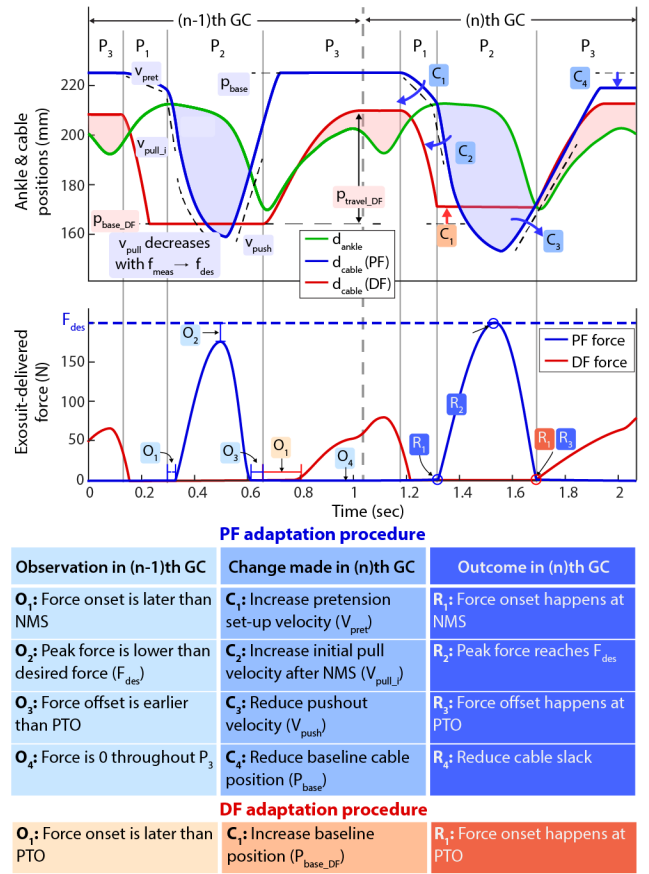where $v(i)$ is a velocity variable in ith gait cycle, $f_{err}(i)$ is a

Figure 7. Illustration of cable position and delivered force trajectories in two consecutive gait cycles (GCs). PF cable position trajectory generator adjusts cable velocities (v_{prt}, v_{pull_i}, and v_{push}) and baseline cable position (p_{base}) for the next GC based on their previous values and force measurements from previous GC. Additionally, cable pull velocity (v_{pull}) is adapted when PF force ramps up to achieve desired peak force (f_{des}). DF trajectory generator also adjust baseline cable position (p_{bae_DF}) to onset DF force at appropriate timings. This illustration demonstrates how the position trajectory generator recovers desired force profile when it observes undesired force profile in the previous GC.

force error between desired and measured values in the ith gait cycle (i.e. $f_{des} - f_{meas}(i)$), and k is a force-velocity adaptation gain. For instance, $v_{pret}(n-1)$ is adjusted based on the difference between desired onset force (7 N) and PF force measured at NMS in ($n-1$)th cycle to generate $v_{pret}(n)$. v_{pull_i} adapts based on the difference of desired peak force and measured peak force. Last, v_{push} is adapted based on the difference of desired offset force (7 N) and force measured at PTO (See Fig. 7 for further details). The adaptation of v_{push} therefore reduces push-out velocity as long as the exosuit does not deliver PF force in paretic swing.

The parameter p_{base} adapts to minimize slack in the cable when PF force is not generated in P3. The adaptation occurs as follows:

$$p_{base}(n) = \begin{cases} p_{base}(n-1) + \Delta p, & f_{max}^{p3}(n-1) > f_{thres} \\ p_{base}(n-1) - \Delta p, & otherwise \end{cases} \qquad (6)$$

where f_{thres} is a force threshold where the algorithm determines if cable force is generated, f_{max}^{p3} is a maximum force measured during P3, and Δp is a position increment. Through this adaptation, p_{base} decreases up to the position

boundary where cable force starts to generate in P3.

Further, the cable velocity (v_{pull}) adapts while PF cable retracts iteratively per each control loop as follows:

$$v_{pull}(t) = v_{pull\_i} \cdot \left(\frac{f_{des}-f_{meas}(t)}{f_{des}-f_{meas\_NMS}}\right) \quad (7)$$

where f_{des} is desired peak force, $f_{meas}(t)$ is a force measurement at each time stamp of control loop, and f_{meas_NMS} is force measurement at NMS, where cable velocity is v_{pull_i}. This with-in stride velocity adaptation increases peak force tracking by decreasing cable velocity as force reaches to f_{des}.

C. DF Cable position trajectory generator

A similar algorithm to PF position trajectory generator was implemented to deliver DF force during paretic swing and weight acceptance (Fig. 7). The algorithm adapts baseline cable position (p_{base_DF}) once per a stride to consistently onset DF force at PTO as follows:

$$p_{base\_DF}(n) = p_{base\_DF}(n-1) + k \cdot f_{err}(n-1) \quad (8)$$

where $f_{err}(n-1)$ is the difference between desired onset force (7 N) and force measurement at PTO in *(n-1)*th gait cycle. A cable travel from p_{base_DF} during swing (p_{travel_DF} in Fig. 7) is manually selected by system operators based on their observation on patients ground clearance and foot landing.

V. SYSTEM VALIDATION

To evaluate the exosuit's performance in assisting walking after stroke, we conducted a preliminary testing with three patients in the chronic phase of stroke recovery (see Table 1). Patients were asked to walk along an overground track equipped with motion capture cameras (Oqus, Qualisys, Sweden) (Fig. 8) for five minutes in three different conditions: first walking without wearing the exosuit (NOEXO), second walking with exosuit using the optimized control algorithm described in this paper (EXO_ON1), and third walking with exosuit using a control algorithm similar to that presented in [17] (EXO_ON2). All the walking trials were supervised by a licensed physical therapist (PT). In walking trials with exosuit, the desired PF peak force (f_{des}) was set at 25% the wearer's body weight (%BW), and p_{travel_DF} was fixed for both conditions. Kinematic data were recorded with the motion capture cameras, and ground reaction force (GRF) data were also recorded with a set of nine instrumented force plates (Bertec CO, USA; sampling frequency 1500 Hz) over a portion on the track. Medical clearance and written informed consent forms approved by the Harvard University Human Subjects Review Board were received from all participants.
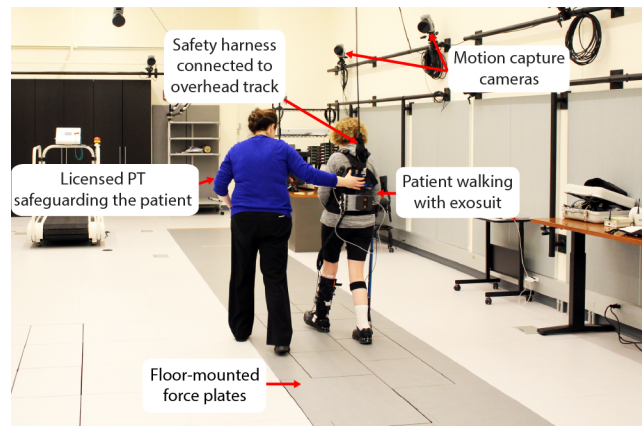

Figure 8. Experimental setup for preliminary system evaluation with patients after stroke.

Joint kinematics were calculated with the inverse kinematics using Visual 3D software (C-Motion Inc, USA). Paretic forward propulsion for each stride was measured as peak anterior GRF (AP GRF) generated by the paretic limb. Of particular interest for performance evaluation were reliability of gait event detection and consistency of peak PF forces, a stated goal of our improved control algorithm. Electrical power consumption of the motor was another performance metric, calculated as

$$p_{motor} = i^2 \cdot R_{motor} + K_i \cdot i \cdot \omega \quad (9)$$

where i is a motor active current, R_{motor} is an effective motor resistance, K_i is a motor constant, and ω is motor angular velocity. Paired-sample t-tests were conducted to compare different walking conditions. The statistical significance level was set at $p < 0.05$. We hypothesized that during overground walking the exosuit would increase paretic forward propulsion and improve paretic dorsiflexion during mid-swing, an important indicator of ground clearance. We also hypothesized that our improved controller would achieve these biomechanical goals with more consistent force profile and reduced motor electric power consumption.

A. Performance evaluation of new gait event detection algorithm

Gait events were also determined via motion capture using an automatic gait event detection algorithm based on ground reaction forces and measured kinematics using Visual 3D software. Synchronizing these events with exosuit data allowed calculation of the error between IMU-detected and actual gait events. For all the subject, average errors were under 90 ms. Specifically, the errors in each participant were: S1: -88.76±6.05 ms; S2: -49.70±8.41 ms; and S3: -49.52±11.96 ms. Negative numbers imply that real time events trailed those determined by motion capture.

TABLE I.   PARTICIPANT BASELINE CHARACTERISTICS AND GAIT PERFORMANCE

Participant No.	Sex	Age (y)	Years after stroke (y)	Paretic side	Weight (kg)	Height (m)	Regular assistive device	Comfortable overground walking speed (m/s)
S1	Male	53	5.0	Left	77.5	184	Foot-up brace & Cane	0.9
S2	Female	64	6.2	Left	78	166	None	1.2
S3	Male	75	5.6	Left	97.5	179	FES	0.8

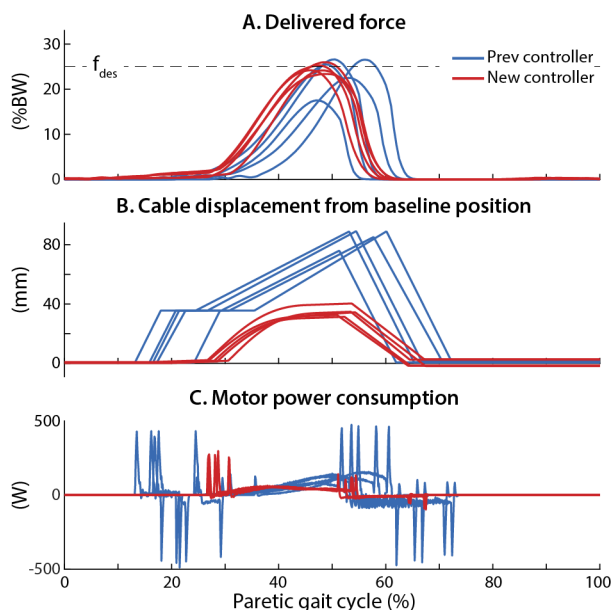FES: Functional Electrical Stimulation device

Figure 9. Sample data to compare old and new PF cable position trajectory generators in (A) delivered force, (B) cable displacement (retraction) from initial baseline position (p_{base}), and (C) motor power consumption. Data from 5 continuous strides in overground walking of a patient after stroke are presented for simplicity.

B. Performance evaluation of new PF cable position trajectory generation algorithm

The averages of peak PF forces achieved using different algorithms were both close to target PF peak force (25%BW) (Fig. 9); However, standard deviations of the peak forces were 70% lower with the new algorithm compared to the previous algorithm (see Table. 2 for individual data). Further, electrical

TABLE II.   PF PEAK FORCE CONSISTENCY (%BW)

Participant No.	Old PF algorithm	New PF algorithm
S1	25.18±2.82	24.97±0.86
S2	25.18±2.54	24.92±1.27
S3	25.19±3.62	24.97±1.08

TABLE III.   AVERAGE ELECTRICAL POWER CONSUMPTION OF PF MOTOR OVER SINGLE STRIDE (W)

Participant No.	Old PF algorithm	New PF algorithm
S1	16.97±2.53	8.29±0.38
S2	11.81±1.29	4.70±0.37
S3	18.10±3.24	10.79±0.76

power consumed by the PF motor significantly reduced with the new algorithm compared to the old algorithm (New: 7.93±3.06 W, Old: 15.63±3.35 W. See table. 3).

C. Biomechanical evaluation

Fig. 10 illustrates the biomechanical responses from individual subjects when walking with the exosuit. Compared to the NO_EXO condition, all three participants increased paretic forward propulsion in the EXO_ON1 condition. Only two participants (S1 and S2) increased paretic forward propulsion in the EXO_ON2 condition. Regarding ground clearance, two participants (S1 and S3) increased their paretic peak dorsiflexion during mid-swing in both EXO_ON1 and EXO_ON2 conditions compared to NOEXO. It should be noted that S2 had the mildest gait impairment in our subject group, presenting good ground clearance in NOEXO condition, therefore did not require increased DF during swing (see Table 1 and Fig. 10). To summarize, with the new control algorithm, the exosuit improved paretic forward propulsion and ground clearance during swing phase, an improvement matching, or even slightly exeeding, the
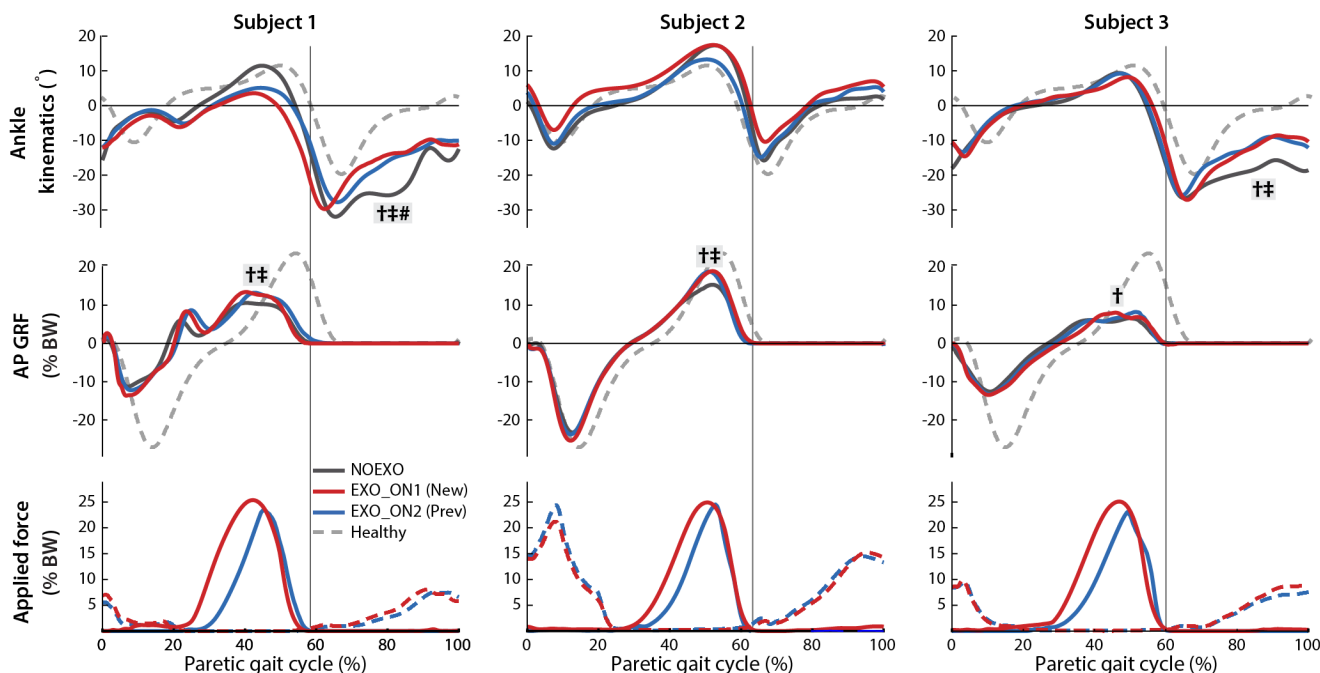

Figure 10. Average biomechanical changes of individual subjects in paretic forward propulsion and ground clearance. (Top) sagittal plane ankle kinematics. (middle) anterior-posterior ground reaction force (AP GRF). (bottom) PF and DF force applied by exosuit. Solid lines are PF forces and dotted lines are DF forces. The vertical lines around 60% GC present paretic toe-off.
* † denotes statistically significant difference between NOEXO and EXO_ON1 condition; ‡ denotes the difference between NOEXO and EXO_ON2 condition: # denotes the difference between EXO_ON1 and EXO_ON2.
** Data collected from healthy individuals walking in 1.5 m/s were presented as a reference.

previous algorithm. Further, the exosuit could deliver better biomechanical outcomes to a patient with a more pronounced gait impairment compared to a mild one. Similar results can be found in [17]. Still, this preliminary validation study is limited by a small sample size, therefore further study including more patients is warranted.

VI. CONCLUSION

This paper presents an optimized soft exosuit for paretic ankle assistance in walking after stroke. The exosuit was designed to improve suitability for translation to clinics by reducing complexity, mass, and volume based on data collected from previous studies with tethered and portable systems [17], [19], [25]. A new control algorithm was implemented to improve gait event detection reliability, PF peak force consistency, and efficiency of motor power consumption, all of which are critical for the use of exosuit in clinical gait training. The exosuit and controller were evaluated through a preliminary experiment with patients poststroke during overground walking, with and without the exosuit. In this experiment, the control algorithm robustly detected PTO, NTO, and NMS and delivered more consistent force profiles, while using 50% lower motor electrical power consumption compared to the prior control algorithm [17]. Similar to what was found in previous studies [17], the patients generated more forward propulsion with the paretic limb and achieved increased ground clearance with improved paretic ankle kinematics during the swing phase. These preliminary results highlight the potential of the exosuit to improve poststroke gait and begin evaluation in larger patient studies.

ACKNOWLEDGMENT

REFERENCES

[1] A. H. A. S. C. and S. S. Subcommittee, "Heart Disease and Stroke Statistics-2017 Update: A Report From the American Heart Association.," *Circulation*, vol. 131, no. 4, pp. e29-322, 2017.

[2] G. E. Gresham, T. E. Fitzpatrick, P. A. Wolf, P. M. McNamara, W. B. Kannel, and T. R. Dawber, "Residual disability in survivors of stroke--the Framingham study.," *N. Engl. J. Med.*, vol. 293, no. 19, pp. 954–956, 1975.

[3] S. Olney and C. Richards, "Hemiparetic gait following stroke. Part I: Characteristics," *Gait Posture*, vol. 4, pp. 136–148, 1996.

[4] K. K. Patterson, I. Parafianowicz, C. J. Danells, V. Closson, M. C. Verrier, W. R. Staines, S. E. Black, and W. E. McIlroy, "Gait asymmetry in community-ambulating stroke survivors.," *Arch. Phys. Med. Rehabil.*, vol. 89, no. 2, pp. 304–310, Feb. 2008.

[5] J. Perry, *Gait Analysis: Normal and Pathological Function*, vol. 12. 2010.

[6] C. L. Peterson, A. L. Hall, S. A. Kautz, R. R. Neptune, E. L. Topp, and J. M. Rosen, "Pre-swing deficits in forward propulsion, swing initiation and power generation by individual muscles during hemiparetic walking.," *J. Biomech.*, vol. 43, no. 12, pp. 2348–2355, Aug. 2010.

[7] S. Nadeau, D. Gravel, A. B. Arsenault, and D. Bourbonnais, "Plantarflexor weakness as a limiting factor of gait speed in stroke subjects and the compensating role of hip flexors.," *Clin. Biomech. (Bristol, Avon)*, vol. 14, no. 2, pp. 125–135, Feb. 1999.

[8] A. L. Hall, C. L. Peterson, S. A. Kautz, and R. R. Neptune, "Relationships between muscle contributions to walking subtasks and functional walking status in persons with post-stroke hemiparesis.," *Clin. Biomech. (Bristol, Avon)*, vol. 26, no. 5, pp. 509–515, Jun. 2011.

[9] P.-Y. Lin, Y.-R. Yang, S.-J. Cheng, and R.-Y. Wang, "The Relation Between Ankle Impairments and Gait Velocity and Symmetry in People With Stroke," *Arch. Phys. Med. Rehabil.*, vol. 87, no. 4, pp. 562–568, Apr. 2006.

[10] V. Weerdesteyn, M. de Niet, H. J. R. van Duijnhoven, and A. C. H. Geurts, "Falls in individuals with stroke.," *J. Rehabil. Res. Dev.*, vol. 45, no. 8, pp. 1195–213, 2008.

[11] Y. Ding, I. Galiana, A. Asbeck, B. Quinlivan, S. M. M. De Rossi, and C. Walsh, "Multi-joint actuation platform for lower extremity soft exosuits," in *Robotics and Automation (ICRA), 2014 IEEE International Conference on*, 2014, pp. 1327–1334.

[12] A. T. Asbeck, S. M. M. De Rossi, K. G. Holt, and C. J. Walsh, "A biologically inspired soft exosuit for walking assistance," *Int. J. Rob. Res.*, pp. 1–19, 2015.

[13] A. T. Asbeck, K. Schmidt, I. Galiana, and C. J. Walsh, "Multi-joint Soft Exosuit for Gait Assistance," in *Robotics and Automation (ICRA), 2015 IEEE International Conference on*, 2015.

[14] B. T. Quinlivan, S. Lee, P. Malcolm, D. M. Rossi, M. Grimmer, C. Siviy, N. Karavas, D. Wagner, A. Asbeck, I. Galiana, and C. J. Walsh, "Assistance magnitude versus metabolic cost reductions for a tethered multiarticular soft exosuit," *Sci. Robot.*, vol. 2, no. 2, p. eaah4416, 2017.

[15] G. Lee, J. Kim, F. A. Panizzolo, Y. M. Zhou, L. M. Baker, I. Galiana, P. Malcolm, and C. J. Walsh, "Reducing the metabolic cost of running with a tethered soft exosuit," *Sci. Robot.*, vol. 2, 2017.

[16] J. Bae, S. M. Maria De Rossi, K. O'Donnell, K. L. Hendron, L. N. Awad, T. R. Teles Dos Santos, V. L. De Araujo, Y. Ding, K. G. Holt, T. D. Ellis, and C. J. Walsh, "A soft exosuit for patients with stroke: Feasibility study with a mobile off-board actuation unit," *Rehabilitation Robotics (ICORR), 2015 IEEE International Conference on.* pp. 131–138, 2015.

[17] L. N. Awad, J. Bae, K. O'Donnell, S. M. M. De Rossi, K. Hendron, L. H. Sloot, P. Kudzia, S. Allen, K. G. Holt, T. D. Ellis, and C. J. Walsh, "A soft robotic exosuit improves walking in patients after stroke," *Sci. Transl. Med.*, vol. 9, no. 400, Jul. 2017.

[18] L. N. Awad, J. Bae, P. Kudzia, A. Long, K. K. Hendron, K. G. Holt, K. O'Donnell, T. D. Ellis, and C. J. Walsh, "Reducing Circumduction and Hip Hiking During Hemiparetic Walking Through Targeted Assistance of the Paretic Limb Using a Soft Robotic Exosuit.," *Am. J. Phys. Med. Rehabil.*, vol. 96, no. 10, pp. 157–164, 2017.

[19] J. Bae, L. Awad, A. Long, K. O. Donnell, K. Hendron, K. G. Holt, T. D. Ellis, and C. J. Walsh, "Biomechanical mechanisms underlying exosuit-induced improvements in walking economy after stroke," *J. Exp. Biol.*, 2018.

[20] D. C. Kerrigan, H. M. Abdulhadi, T. A. Ribaudo, and U. Della Croce, "Biomechanic effects of a contralateral shoe-lift on walking with an immobilized knee," *Arch. Phys. Med. Rehabil.*, vol. 78, no. 10, pp. 1085–1091, 1997.

[21] G. Lee, Y. Ding, I. G. Bujanda, N. Karavas, Y. M. Zhou, and C. J. Walsh, "Improved assistive profile tracking of soft exosuits for walking and jogging with off-board actuation," in *2017 IEEE/RSJ International Conference on Intelligent Robots and Systems (IROS)*, 2017, pp. 1699–1706.

[22] R. C. Browning, J. R. Modica, R. Kram, and A. Goswami, "The effects of adding mass to the legs on the energetics and biomechanics of walking," *Med. Sci. Sports Exerc.*, vol. 39, no. 3, pp. 515–525, 2007.

[23] B. Quinlivan, A. Asbeck, D. Wagner, T. Ranzani, S. Russo, and C. J. Walsh, "Force Transfer Characterization of a Soft Exosuit for Gait Assistance," *Vol. 5A 39th Mech. Robot. Conf.*, p. V05AT08A049, 2015.

[24] H. Lau and K. Tong, "The reliability of using accelerometer and gyroscope for gait event identification on persons with dropped foot," *Gait Posture*, vol. 27, no. 2, pp. 248–257, 2008.

[25] L. N. Awad, D. S. Reisman, R. T. Pohlig, and S. A. Binder-Macleod, "Reducing The Cost of Transport and Increasing Walking Distance After Stroke," *Neurorehabil. Neural Repair*, vol. 30, no. 7, pp. 661–670, Aug. 2016.